

Anisotropic hopping conduction in spin-coated PEDOT:PSS thin films

A. M. Nardes, M. Kemerink, and R. A. J. Janssen

Department of Applied Physics, Eindhoven University of Technology, P.O. Box 513, 5600 MB Eindhoven, The Netherlands

(Received 21 May 2007; published 20 August 2007)

The charge transport in spin-coated poly(3,4-ethylenedioxythiophene):poly(styrenesulfonate) (PEDOT:PSS) has been investigated as a function of temperature and electric field. Both the magnitude and the transport mechanism are found to be strongly anisotropic. This striking behavior is quantitatively explained in terms of a morphological model in which flattened, quasimetallic PEDOT-rich grains are organized in horizontal layers that are separated by continuous insulating PSS lamellas. In this model, the in-plane conductivity is described by three-dimensional variable range hopping between ~ 25 nm sized PEDOT-rich particles separated by subnanometer PSS barriers, while the out-of-plane conductivity is described by nearest-neighbor hopping between more widely spaced molecular sites. These length scales are supported by previously reported scanning probe measurements.

DOI: [10.1103/PhysRevB.76.085208](https://doi.org/10.1103/PhysRevB.76.085208)

PACS number(s): 73.61.Ph, 73.50.Fq, 72.20.Ee

I. INTRODUCTION

Conducting polymers offer a unique combination of properties that makes them attractive materials for many electronic applications. Typically, these polymers are made conducting by chemical doping, resulting in polycations or polyanions with a relatively mobile charge.¹ The conductivity of these materials can be tuned by, amongst others, chemical manipulation of the polymer backbone, the nature of the dopant, the degree of doping, and by blending with other polymers.

Poly(3,4-ethylenedioxythiophene) blended with poly(4-styrenesulfonic acid) (PEDOT:PSS) is one of the most important and successful conducting polymers synthesized in the field of organic electronics.² The combination of a relatively high conductivity³ with optical transparency in the doped state makes PEDOT:PSS suitable for applications such as antistatic coatings,⁴ electrode in light-emitting diodes,⁵ photovoltaics,⁶ memories,⁷ sensors,⁸ and as active material for electrochromic devices.⁹ As such, PEDOT:PSS has found application in basically all organic and/or polymeric devices. Even though there is extensive commercial and scientific interest in PEDOT:PSS, the nature of the charge transport is still not clear. In addition, the correlation between the morphology and the conductive properties is incompletely understood and has been addressed in a limited number of publications.^{10–15}

Despite large differences in interpretation and experimental data, it is generally believed that charge transport in PEDOT:PSS occurs by a hopping process. Typically, the resulting conductivity σ can be described by

$$\sigma(T) = \sigma_0 \exp \left[- \left(\frac{T_0}{T} \right)^\alpha \right], \quad (1)$$

where T_0 is a material-dependent parameter and the exponent $\alpha = 1/(1+D)$ is taken as the signature of variable range hopping¹⁶ (VRH) in D dimensions. Alternatively, an exponent close to $1/2$ can result from the effects of either Coulomb interactions that cause the opening of a soft gap in the density of states¹⁷ or charging energy in a granular (quasi-)metallic system.^{18,19}

From the few papers addressing the charge transport in PEDOT:PSS systems, no consistent picture emerges. For instance, some authors^{20–22} have interpreted the temperature dependence of the conductivities of pristine PEDOT:PSS thin films in terms of a one-dimensional VRH model with $\alpha = 1/2$. On the other hand, Aleshin *et al.*³ interpreted $\alpha = 1/2$ on freestanding pristine PEDOT:PSS thick films in terms of a charging energy model^{18,19} proposed by Zuppiroli *et al.*²³ In this model, conduction is supposed to result from tunneling between small conducting grains separated by an insulating barrier. Such a model seems reasonable to explain electronic conduction in PEDOT:PSS thin films since the morphology of it is supposed to be a phase segregated material consisting of conductive PEDOT-rich grains surrounded by a shell formed by excess PSS,²⁴ which is only weakly (ionically) conducting and acts as an insulating barrier. However, in this model, a particular relation between shell thickness and core diameter of the particles is required, for which, in the case of PEDOT:PSS, no experimental indications are found.¹²

Recently, more detailed insights in the morphology of PEDOT:PSS have been obtained. Conductive atomic force microscopy (AFM) experiments micrometer-thick drop cast PEDOT:PSS films have suggested that the morphological model for PEDOT:PSS thin films is actually a lamellar structure of PEDOT and PSS.¹⁰ In our previous work,¹² the lamellar structure was confirmed and resolved in more detail for spin-coated thin films by phase-sensitive AFM on cryogenically cleaved PEDOT:PSS samples, which revealed a cross-sectional view of the morphology. From that, it was found that the PEDOT-rich oblate-spheroid- or pancake-shaped particles, 20–30 nm in diameter (d_{\parallel}) and 4–6 nm in height (d_{\perp}), are actually organized in layers that are separated by quasicontinuous nanometer-thick PSS lamellas (see Fig. 1 for a schematic representation). The morphology qualitatively explained the observed differences in magnitude and temperature dependences of the conductivity in the normal (\perp) and parallel (\parallel) current directions. Particularly, it was shown that the conductivities of spin-coated PEDOT:PSS thin films, measured in lateral and vertical directions with respect to the sample surface, are highly anisotropic in the temperature range of 77–300 K and are well described by

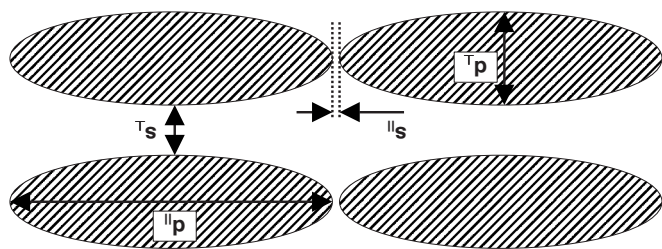


FIG. 1. Schematic representation of the morphological model for PEDOT:PSS (side view). Quasimetallic PEDOT-rich clusters (hatched regions) are separated by lamellas of insulating PSS (gray background).

Eq. (1).¹² In the normal direction, the horizontal PSS lamellas were assumed to impose nearest-neighbor^{16,17} hopping (nn-H) between the quasimetallic PEDOT particles, leading to a strongly reduced conductivity and a temperature exponent $\alpha=1$. The exponent $\alpha=1/4$ that is observed for lateral transport was tentatively attributed to VRH^{16,17} between the PEDOT-rich particles that are laterally separated by much thinner barriers, leading to an enhanced conductivity in this direction.

The present investigation is motivated by the need to quantify this model. In particular, the question raised is what is the nature of the states between which the hopping takes place? Are these individual (sub)nanometer-sized molecular sites formed by, e.g., single ionized PEDOT segments, or are these PEDOT-rich particles that contain many, strongly coupled ionized PEDOT segments? We will show results of the electric field dependence measurements (non-Ohmic hopping conduction) where the characteristic hopping lengths for vertical (L_{\perp}) and lateral (L_{\parallel}) transport are extracted and found to agree very well with the expectations for VRH and nn-H transport. Based on the L_{\parallel} values, it will be demonstrated that the hopping process takes place between PEDOT-rich islands and not between single PEDOT segments or dopants. The constant L_{\perp} values indicate hopping within and through the insulator PSS barrier. In the end, these results are combined in a morphological model that is fully consistent with earlier findings¹² and accounts quantitatively for all parameters involved in the charge transport.

II. EXPERIMENT

The sample substrates consisted of $3 \times 3 \text{ cm}^2$ soda lime glass, optionally covered with indium tin oxide (ITO) with a specific sheet resistance of $15 \Omega/\square$, and were cleaned in ultrasonic baths of acetone and isopropanol for 20 min each and rinsed with de-ionized water in between. Residual organic contaminations were removed using a 30 min UV-ozone treatment (UV-Ozone Photoreactor, PR-100, Ultraviolet Products).

For the in-plane (lateral, \parallel) electrical measurements, four electrodes ($1 \times 6 \text{ mm}^2$, 1 mm apart from each other) of 5 nm of chromium followed by 95 nm of gold were evaporated on top of cleaned bare glass substrates. For the out-of-plane (vertical, \perp) electrical measurements, 100 nm of gold were evaporated on top of the ITO to eliminate the spurious series

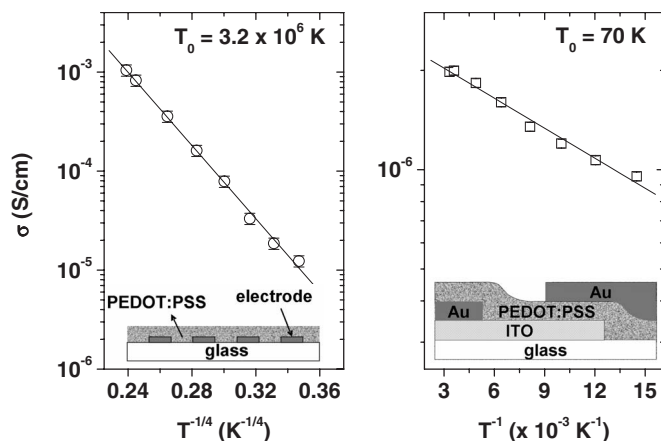


FIG. 2. Symbols represent conductivity vs (a) T^{-1} and (b) T^{-1} for PEDOT:PSS samples measured in lateral (\parallel) and vertical directions (\perp), respectively. Straight lines are fits to Eq. (1). The insets show the devices used. The bottom gold layer in the vertical device shunts the ITO underneath, which has a much higher resistivity. Electrical contacts are made to both gold pads, which have a lateral separation of less than 1 mm.

resistance caused by the ITO (see insets of Fig. 2). The PEDOT:PSS solution, purchased from Starck by the trade name of Baytron P VP Al 4083,²⁵ was filtered using a $5 \mu\text{m}$ filter and deposited in air by spin coating for both types of electrode geometries. Then, samples were transferred into a glovebox (O_2 and $\text{H}_2\text{O} < 1 \text{ ppm}$) and subsequently annealed on a hot plate at $200 \text{ }^\circ\text{C}$ for 2 min to remove water. The final film thickness was about 60 nm as measured by a profilometer (Alpha-step 200, Tencor Instruments). The remaining top contact for the \perp electrode geometry sample was made by the evaporation of 100 nm of gold on top of the PEDOT:PSS thin film using a shadow mask which is aligned just next to the bottom Au layer, giving an active area of 0.35 cm^2 . After cutting the desired sample from the substrate, it was placed inside a cryostat (Oxford Instruments), evacuated to 10^{-5} mbar and brought to the desired temperature in the 77–300 K range. Temperature control was provided by an Oxford ITC 601 temperature controller that maintained temperature stability within $\pm 0.1 \text{ K}$. Electrical measurements were performed by a semiconductor parameter analyzer (Agilent model 4156C). For all temperature-dependent measurements, the electrical connections were made inside the glovebox, so the measured samples never experienced contact with air after bakeout. From a comparison of two- and four-terminal measurements, the contact resistance was found to be negligible for all our samples.

III. RESULTS

A. Temperature dependence

The temperature dependencies of the conductivity $\sigma(T)$ in the Ohmic or low electric field regime for the spin-coated PEDOT:PSS thin films measured in lateral and vertical directions are shown in Figs. 2(a) and 2(b).²⁶

Two remarkable features are observed in Fig. 2: first, the large difference in magnitude of σ , and second, the different

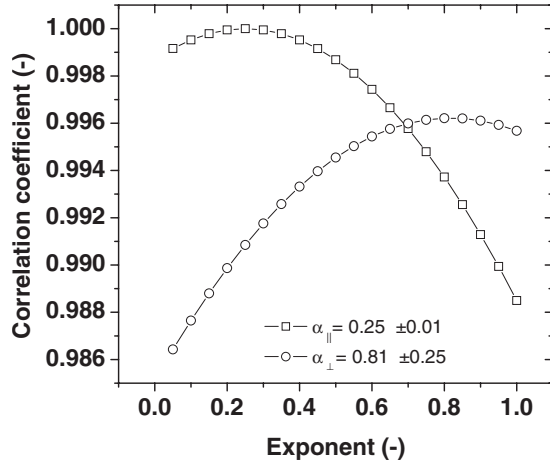


FIG. 3. Correlation coefficients of the measured and fitted [using Eq. (1)] conductivities versus exponent α for PEDOT:PSS samples measured in lateral (\parallel) and vertical directions (\perp) over 77–300 K.

temperature dependence of σ , as observed by the different values of α for \parallel and \perp directions. Since α is the main parameter to give information about the conduction mechanism and the measured temperature-dependent data of any material may exhibit, within experimental error, visually good and indistinguishable linearity on $\log \sigma(T)$ vs T^α plots for “any” α value between 0.1 and 1 over the entire temperature range, its precise value is of major importance. In Fig. 3, the correlation coefficient of the fit of Eq. (1) to the measured conductivity is plotted against α . The maxima are $\alpha_{\parallel} = 0.25 \pm 0.01$ ($R = 0.99999$) and $\alpha_{\perp} = 0.81 \pm 0.25$ ($R = 0.99621$), close to the theoretical values of $1/4$ for three-dimensional (3D) VRH and of 1 for nn-H. Using α equal to $1/4$, we find the fitting parameters of Eq. (1) for the \parallel direction as the slope $T_{0,\parallel} = (3.2 \pm 0.1) \times 10^6$ K and $\sigma_0 = (24.6 \pm 1.3)$ S/cm. In this case, $T_{0,\parallel} = \beta / N(E_F) \xi_{\parallel}^3 k_B$, where β (~ 21.2) (Ref. 17) is a numerical factor, k_B is the Boltzmann constant, and ξ_{\parallel}^3 is the effective localization length.²⁷

In the \perp direction, the activation energy is the slope $E_3 = k_B T_{0,\perp} \sim 1 / N(E_F) a^3$, with a the average intersite distance (roughly equal to the cube root of the site density), giving $\sigma_0 = (2.6 \pm 1.1) \times 10^{-6}$ S/cm and $E_3 = (6.0 \pm 0.5) \times 10^{-3}$ eV which corresponds to $T_{0,\perp} = 70$ K. In this case, the parameter E_3 represents the typical intersite energy difference.

B. Electric field dependence

We turn our attention now to the electric field dependence measurements, which enable one to extract the length scales of the predominant transport process.^{28,29} As the applied electric field approaches zero, σ approaches a constant value which depends on the temperature, i.e., the Ohmic regime is entered. In the opposite case, as the electric field is increased, deviations from Ohmic behavior become apparent and one expects an increase in σ when the energy associated with the electric field times a typical hopping distance becomes of the same order as the typical intersite energy difference.

1. Normal direction

For nn-H in a disordered material, as observed here in the \perp direction, we first derive an expression to quantify the non-Ohmic conductivity. We demand that the current is symmetrically modified by forward and reverse fields, i.e., the field modifies the forward and reverse hopping probabilities by equally lowering and raising the energy required for typical forward and reverse hops. This directly leads to the following equation for the vertical current density J_{\perp} :

$$J_{\perp}(F, T) \propto \exp\left[-\frac{E_3}{k_B T}\right] \left\{ \exp\left(\frac{eF_{\perp}L_{\perp}}{k_B T}\right) - \exp\left(-\frac{eF_{\perp}L_{\perp}}{k_B T}\right) \right\} \propto \left\{ 2 \sinh\left(\frac{eF_{\perp}L_{\perp}}{k_B T}\right) \right\}, \quad (2)$$

where E_3 is the activation energy, $eF_{\perp}L_{\perp}/k_B T$ is the amount by which forward and reverse energies are lowered and raised, and e is the electron charge. F_{\perp} and L_{\perp} are the applied electric field and the characteristic nearest-neighbor hopping length in the \perp direction, respectively.

In Eq. (2), by expanding the sinh function as $x + (x^3/3!) + \dots + [x^{2n+1}/(2n+1)!]$ and combining with $\sigma = J/F$, we find for the electric field dependence of conductivity at modest fields, i.e., $eF_{\perp}L_{\perp}/k_B T < 1$:

$$\sigma_{\perp}(F, T) \propto \sigma_{0,\perp}(0, T) \left[1 + \frac{1}{6} \left(\frac{eF_{\perp}L_{\perp}}{k_B T} \right)^2 \right]. \quad (3)$$

The experimental dependence of the conductivity on field strength is shown in Fig. 4(a) for the \perp direction. The conductivity increases with the applied electric field F and such behavior is more pronounced at lower temperatures.

In Fig. 4(a), the solid lines are fits to Eq. (3), and the slopes of σ vs F/T curves for $F \rightarrow 0$, which give L_{\perp} , were extracted and plotted in Fig. 4(b). Despite the relatively large scatter and the magnitude of the error bars, Fig. 4(b) shows the absence of a clear trend in $L_{\perp}(T)$, in agreement with nn-H theory.^{16,17} Taking a equal to $L_{\perp} = 1.4$ nm and $T_0 = 70$ K, we find $N(E_F)_{\perp} = 6.0 \times 10^{22}$ eV $^{-1}$ cm $^{-3}$.

2. Lateral direction

Several authors derived expressions for the field dependence of the current in 3D VRH at modest fields, i.e., when $eF_{\parallel}L_{\parallel}/k_B T < 1$. Ladiou *et al.*³⁰ have summarized the 3D VRH current equation for modest electric fields as follows:

$$I_{\parallel}(F, T) = I_{0,\parallel} \exp\left\{ -\left(\frac{T_0}{T}\right)^{\alpha} \left[1 - A \frac{(eF_{\parallel}\xi_{\parallel}')^x}{(k_B T)^{x'}} + B \left(\frac{eF_{\parallel}\xi_{\parallel}'}{k_B T}\right)^{\beta} \right] \right\}, \quad (4)$$

where A , B , x , x' , and β are parameters, A and B being positive. The first term $A(eF_{\parallel}\xi_{\parallel}')^x/(k_B T)^{x'}$ represents the enhancement of the hopping probability when F grows. The second term $B(eF_{\parallel}\xi_{\parallel}')/k_B T$ was only addressed by Böttger *et al.*³¹ and arises when the presence of reverse hops or “returns” in the optimal percolation pathway is taken into account.³¹ When the field increases, these trajectories rapidly lose probability, which prevents the current from increasing

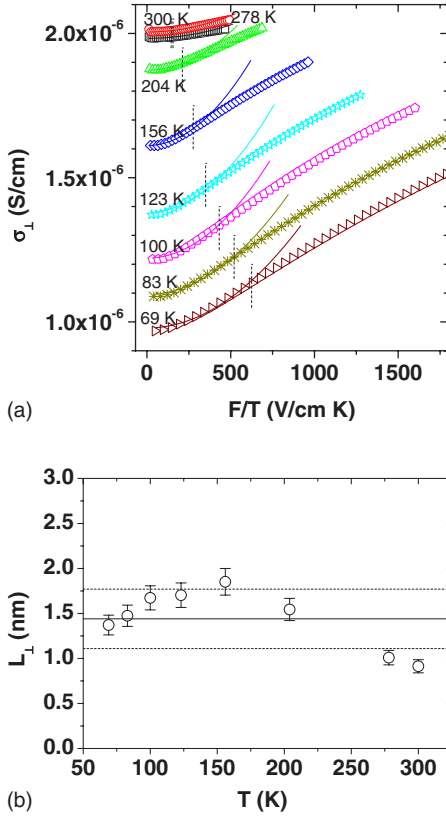


FIG. 4. (Color online) (a) Conductivity vs F/T for PEDOT:PSS thin film measured in vertical (\perp) direction with respect to the film plane at different temperatures. Solid lines are fits to Eq. (3). (b) Temperature dependence of the characteristic hopping length L_{\perp} for the same sample. $L_{\perp} = (1.4 \pm 0.4)$ nm.

too quickly and may actually lead to a negative differential conductivity. At somewhat higher fields, this term becomes irrelevant, and under typical experimental conditions, Eq. (4) converges to^{29–32}

$$\sigma_{\parallel}(F, T) = \sigma_{0,\parallel}(0, T) \exp\left(0.17 \frac{eF_{\parallel}L_{\parallel}}{k_B T}\right), \quad (5)$$

where F_{\parallel} is the applied electric field and L_{\parallel} the characteristic hopping length. Note that Eq. (5) results from Eq. (4) by neglecting the returns ($B=0$) and by assuming that the F_{\parallel} and T dependencies of σ_{\parallel} and I_{\parallel} are close to each other. An expression similar to Eq. (5) was derived by Shklovskii *et al.*, who ignored correlations between site energies²⁹ but took field-induced changes in the local chemical potential into account,³³ giving $A \approx 1$, $x = x' = 0.53$, and $B=0$ in Eq. (4). In order to limit the number of free parameters, we shall first use Eq. (5) to describe the “high” field data and subsequently use these parameters as input in Eq. (4) to interpret our full results.

At each temperature in Fig. 5(a), the data are fitted quite well by straight lines, using Eq. (5). Indeed, the nonzero slope of σ_{\parallel} vs F/T in the entire field range shown indicates that there is an electric-field-induced nonlinearity in σ_{\parallel} and this behavior, as for the \perp direction, is more pronounced at low temperatures.

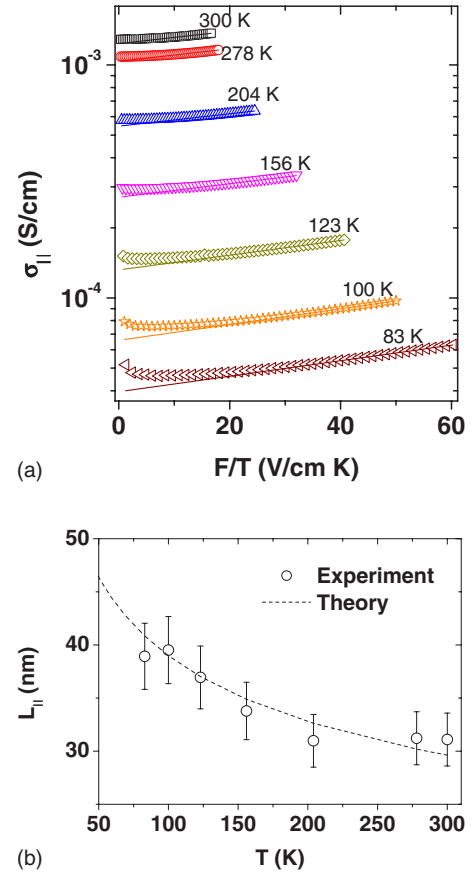


FIG. 5. (Color online) (a) Conductivity vs F/T for PEDOT:PSS thin film measured in lateral (\parallel) direction with respect to the film plane at different temperatures. Solid lines are fits to Eq. (5). (b) Temperature dependence of the characteristic hopping length L_{\parallel} for the same sample.

As the temperature is changed, the slope of the lines through the data in Fig. 5(a) also changes, implying that the characteristic hopping length L_{\parallel} , in contrast to L_{\perp} , is temperature dependent, in agreement with VRH theory. Figure 5(b) shows a plot of the temperature dependence of L_{\parallel} . The characteristic hopping length in 3D VRH is expected to vary as $T^{-1/4}$ at low temperatures. By combining $T_0 = \beta/N(E_F)\xi_{\parallel}^{\prime 3}k_B$ and the Mott expression for $L_{\parallel} = [(8\pi/9)k_B T N(E_F)/\xi_{\parallel}^{\prime}]^{-1/4}$,³⁴ we arrive at

$$\frac{L_{\parallel}}{\xi_{\parallel}^{\prime}} = \left[\frac{9}{8\pi\beta}\right]^{1/4} \left[\frac{T_0}{T}\right]^{1/4}, \quad (6)$$

which is used to fit the experimental data of L_{\parallel} by adjusting the term ξ_{\parallel}^{\prime} [dashed line in Fig. 5(b)]. Clearly, the experiment is well described by the theoretical prediction and ξ_{\parallel}^{\prime} was found to be (8.2 ± 0.5) nm. Using this result and the expression for $T_{0,\parallel}$, $N(E_F)_{\parallel}$ is found to be $1.4 \times 10^{17} \text{ eV}^{-1} \text{ cm}^{-3}$. Most importantly, the magnitude of the characteristic hopping length in the lateral direction is fully consistent with hopping transport between ~ 25 nm sized particles rather than with hopping between individual molecular sites.

TABLE I. Parameters describing the electrical conduction in Baytron P PEDOT:PSS thin films. See text for further discussion.

	Lateral (\parallel)	Vertical (\perp)
Conduction mechanism	3D-VRH	nn-H
σ at 300 K (S/cm)	$(1.1 \pm 0.1) \times 10^{-3}$	$(2.0 \pm 0.1) \times 10^{-6}$
T_0 (K)	$(3.2 \pm 0.1) \times 10^6$	70 ± 6
σ_0 (S/cm)	24.7 ± 1.3	$(2.6 \pm 1.1) \times 10^{-6}$
$N(E_F)$ (eV cm^3) $^{-1}$	$(1.4 \pm 0.2) \times 10^{17}$	$(6.0 \pm 1.7) \times 10^{22}$
ξ' (nm)	8.2 ± 0.5	
L (nm)	30–40	1.4 ± 0.4

IV. DISCUSSION

In this section, we will first evaluate the length scales and density of states that were extracted in the preceding section and, where possible, relate them to the morphological model that was outlined in the Introduction. Second, we will discuss the discrepancies between the experimental and fitted conductivities in Figs. 4(a) and 5(a).

The use of an effective localization length ξ'_{\parallel} , instead of the normal one which appears in conventional Mott theory, is common practice in granular systems.²⁷ The underlying argument is that the only *significant* decay of the wave function occurs in the separating barriers, i.e., in the quasi-insulating PSS and not in the quasimetallic PEDOT-rich particles. This implicitly requires a strong coupling between the wave functions of the individual PEDOT sites. Given the high degree of doping—about one in three PEDOT monomers is ionized³⁵—and the high PEDOT density in the cores (the cores take up less than half the film volume¹²), the fulfillment of this requirement is not at all unlikely.²³ Under this condition, the relation between the effective localization length and the decay length in the barrier ξ can be approximated by $\xi'_{\parallel} = \xi(d_{\parallel} + s_{\parallel})/s_{\parallel}$, with d_{\parallel} and s_{\parallel} the particle diameter and spacing as defined in Fig. 1. The absence of an accurate measure of s_{\parallel} prevents a precise calculation of ξ , but taking s_{\parallel} between 0.5 and 1 nm and $d_{\parallel} = 25$ nm, a value of ξ in the range of 0.15–0.3 nm is found, which again seems reasonable.²³

Turning now to the density of states, we observe that the experimentally extracted value in Table I, $N_{\parallel}(E_F) = 1.4 \times 10^{17} \text{ eV}^{-1} \text{ cm}^{-3}$, corroborates the physical picture sketched in the preceding paragraph. Assuming a rectangular density of states with a typical width of 0.5 eV and a volume per site of $25 \times 25 \times 6 \text{ nm}^3$, the morphological model leads to a density of states of roughly $1.3 \times 10^{17} \text{ eV}^{-1} \text{ cm}^{-3}$, in excellent agreement with the value derived from transport measurements.

The large and unexpected difference between $N_{\parallel}(E_F)$ and $N_{\perp}(E_F)$ of ~ 5 orders of magnitude indicates that the sites that dominate the transport are not the same for both directions. In addition, the value of 1.4 nm found for a is in contradiction with nearest-neighbor hopping between PEDOT-rich particles. In the latter case, a value of 5–6 nm should be observed. Therefore we have to conclude that the dominating nn-H process is, in fact, taking place between dilute states inside the insulating PSS lamellas.

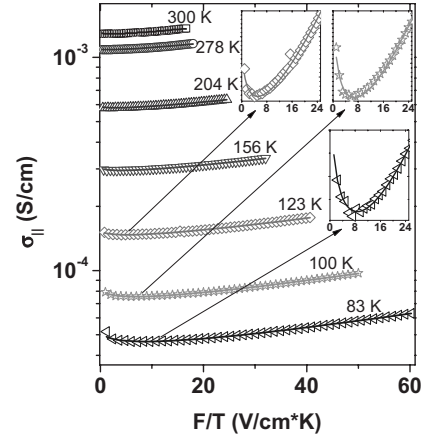


FIG. 6. Conductivity vs F/T for a PEDOT:PSS film measured in lateral (\parallel) direction with respect to the film plane at different temperatures. Solid lines are fits to Eq. (4), considering the presence of reverse hops or returns in the optimal percolation pathway. The insets show the same conductivity vs F/T plots for sample at 83, 100, and 123 K, restricted to low electric fields.

These results are fully consistent with our previous, qualitative analysis on similar samples,¹² and we conclude that the temperature and field dependencies of the anisotropic conductivity in spin-coated PEDOT:PSS thin films are in full quantitative agreement with the morphological model proposed in Ref. 12.

Let us now go back to the deviations from the theoretically predicted field dependence in Figs. 4(a) and 5(a). In the vertical direction [Fig. 4(a)], the conductivity is found to increase slower than quadratically beyond a certain field strength. The critical field F_c at which this sets in is given by the ratio of the energy difference E_3 and tunneling distance a associated with a typical hop, i.e., $E_3 = k_B T_0 \approx eaF_c$. The vertical lines in Fig. 4(a) indicate the position of F_c for various curves. As expected, once the critical field is reached, the differential conductivity decreases.

Finally, we return to the problem of the returns in the lateral conductivity. The problem is extremely complex, and the precise values of the parameters in Eq. (4) were found to depend on the assumptions made. For example, Shklovskii³³ takes into account changes in the chemical potential by the field, giving $A \sim 1$ and $x = x' \sim 0.53$ in Eq. (4), whereas Pollak and Riess²⁹ take into account the correlations between nearest-neighbor sites, giving $x = x' = 1$ and $A = 0.085$ in Eq. (4). For both models, however, the returns, i.e., the second term in Eq. (4), are neglected. In the few theoretical works dealing with this problem, Böttger *et al.* have found by numerical calculation³¹ $x = x' = 1$, $A = 1/6$, $B \sim 0.02$, and $\beta \sim 0.9$, with β a parameter related to the return length, with 50% of error due to numerical uncertainties. In order to assess this behavior in our samples, we therefore replot Fig. 5(a) into Fig. 6, and for each temperature, a fitting to Eq. (4) has been performed using as fixed parameters the ones previously obtained, i.e., T_0 , α , ξ'_{\parallel} , and $x = x' = 1$.

In the investigated temperature range, we found that the Pollak-Riess model best describes our data, yielding in the second term of Eq. (4) $B = 0.02 - 0.05$ and $\beta = 0.36 - 0.60$, not

so far from the values found by Böttger *et al.*³¹ Because of the various uncertain numerical factors involved in the theoretical works, we refrain from making an estimation of the actual length of the returns. However, taking into account the second term of Eq. (4), a distinctly better description of the data is obtained, especially at low electric field and temperature (see insets of Fig. 6 for 83, 100, and 123 K, where this behavior is more pronounced). Qualitatively, these results show that a considerable rearrangement of the percolation pathways occurs in these samples at relatively low field strengths. The convergence of the data to the description by Pollak and Riess²⁹ [Eq. (4)] indicates that at intermediate fields the percolation pathways are more or less fixed in space.

V. CONCLUSIONS

The presented results allow us to set a quantitative morphological model for PEDOT:PSS thin films that, on the one hand, incorporates all length scales that are found in the field dependent measurements and, on the other hand, is fully con-

sistent with previously reported scanning probe data¹² (see Fig. 1). In the \perp direction, the separating PSS barriers are (quasi)continuous and 1–2 nm thick, whereas the separations in the \parallel direction are, on average, much thinner, i.e., $s_{\perp} \gg s_{\parallel}$. Due to this particular morphology, spin cast films of PEDOT:PSS have a relatively high in-plane conductivity, which is well described by 3D variable range hopping. In the out-of-plane direction, the low site density in the PSS enforces nearest-neighbor hopping and an up to 3 orders of magnitude lower conductivity.

ACKNOWLEDGMENTS

We thank Reinder Coehoorn and Margreet de Kok of Philips Research Laboratories for their continuing interest and constructive comments. We also thank Albert van Bree-men, Nicole Kiggen, Jolanda Bastiaansen, and Bea Langeveld of TNO Science and Industry for generously providing materials and samples and for fruitful discussions. A.M.N. acknowledges the Alþan Program (the European Union Programme of High Level Scholarships for Latin America, ID No. E03D19439BR) for financial support.

¹*Handbook of Conducting Polymers*, edited by T. A. Skotheim and J. Reynolds, 3rd ed. (CRC, Boca Raton, FL, 2007).

²L. B. Groenendaal, F. Jonas, D. Freitag, H. Pielartzik, and J. R. Reynolds, *Adv. Mater. (Weinheim, Ger.)* **12**, 481 (2000); S. Kirchmeyer and K. Reuter, *J. Mater. Chem.* **15**, 2077 (2005).

³A. N. Aleshin, S. R. Williams, and A. J. Heeger, *Synth. Met.* **94**, 173 (1998).

⁴F. Jonas, W. Krafft, and B. Muys, *Macromol. Symp.* **100**, 169 (1995).

⁵M. M. de Kok, M. Buechel, S. I. E. Vulto, P. van de Weijer, E. A. Meulenkaamp, S. H. P. M. de Winter, A. J. G. Mank, H. J. M. Vorstenbosch, C. H. L. Weijtens, and V. van Elsbergen, *Phys. Status Solidi A* **201**, 1342 (2004).

⁶C. J. Ko, Y. K. Lin, F. C. Chen, and C. W. Chu, *Appl. Phys. Lett.* **90**, 063509 (2007).

⁷F. Verbakel, S. C. J. Meskers, and R. A. J. Janssen, *Chem. Mater.* **18**, 2707 (2006).

⁸S. C. J. Meskers, J. K. J. van Duren, R. A. J. Janssen, F. Louwet, and L. Groenendaal, *Adv. Mater. (Weinheim, Ger.)* **15**, 613 (2003).

⁹A. Kumar, D. M. Welsh, M. C. Morvant, F. Piroux, K. A. Ab-boud, and J. R. Reynolds, *Chem. Mater.* **10**, 896 (1998).

¹⁰C. Ionescu-Zanetti, A. Mechler, S. A. Carter, and R. Lal, *Adv. Mater. (Weinheim, Ger.)* **16**, 385 (2004).

¹¹S. Timpanaro, M. Kemerink, F. J. Touwslager, M. de Kok, and S. Schrader, *Chem. Phys. Lett.* **394**, 339 (2004).

¹²A. M. Nardes, M. Kemerink, R. A. J. Janssen, J. A. M. Bas-tiaansen, N. M. M. Kiggen, B. M. W. Langeveld, A. J. J. M. van Breemen, and M. M. de Kok, *Adv. Mater. (Weinheim, Ger.)* **19**, 1196 (2007).

¹³X. Crispin, F. L. E. Jakobsson, A. Crispin, P. C. M. Grim, P. Anderson, A. Volodin, C. van Haesendonck, M. Van der Auw-erker, W. R. Salaneck, and M. Berggren, *Chem. Mater.* **18**, 4354

(2006).

¹⁴J. Huang, P. F. Miller, J. S. Wilson, A. J. de Mello, J. C. de Mello, and D. D. C. Bradley, *Adv. Funct. Mater.* **14**, 562 (2005).

¹⁵T. Y. Kim, J. E. Kim, and K. S. Suh, *Polym. Int.* **55**, 80 (2006).

¹⁶N. Mott and E. A. Davis, *Electronic Processes in Non-Crystalline Materials* (Clarendon, Oxford, 1979).

¹⁷B. I. Shklovskii and A. L. Efros, *Electronic Properties of Disor-dered Semiconductors* (Springer, Berlin, 1984).

¹⁸P. Sheng, B. Abeles, and Y. Arie, *Phys. Rev. Lett.* **31**, 44 (1973).

¹⁹P. Sheng, *Phys. Rev. B* **21**, 2180 (1980).

²⁰J. Y. Kim, J. H. Jung, D. E. Lee, and J. Joo, *Synth. Met.* **126**, 311 (2002).

²¹J. Ouyang, Q. Xu, C. W. Chu, Y. Yang, G. Li, and J. Shinar, *Polymer* **45**, 8443 (2004).

²²S. Ashizawa, R. Horikawa, and H. Okuzaki, *Synth. Met.* **153**, 5 (2005).

²³L. Zuppiroli, M. N. Bussac, S. Paschen, O. Chauvet, and L. Forro, *Phys. Rev. B* **50**, 5196 (1994).

²⁴X. Crispin, S. Marciniak, W. Osikowicz, G. Zotti, A. W. Denier van der Gon, F. Louwet, M. Fahlman, L. Groenendaal, F. de Schryver, and W. R. Salaneck, *J. Polym. Sci., Part B: Polym. Phys.* **41**, 2561 (2003).

²⁵<http://www.baytron.com>; http://www.baytron.com/pages/985/physical_properties.pdf

²⁶The values of the parameters T_0 and σ_0 are found to depend on the batch of material used and on the age of the batch. These variations in T_0 and σ_0 are typically less than a factor of ~ 2 and ~ 10 , respectively. Variations between samples prepared in one day are typically below 10% for both parameters. The values of α do not vary with batch or sample.

²⁷J. Zhang and B. I. Shklovskii, *Phys. Rev. B* **70**, 115317 (2004).

²⁸R. M. Hill, *Philos. Mag.* **24**, 1307 (1971).

²⁹M. Pollak and I. Riess, *J. Phys. C* **9**, 2339 (1976).

- ³⁰F. Ladieu, D. L'Hôte, and R. Tourbot, *Phys. Rev. B* **61**, 8108 (2000).
- ³¹H. Böttger and D. Wegener, *Phys. Status Solidi B* **121**, 413 (1984); H. Böttger and V. V. Bryksin, *Hopping Conduction in Solids* (VCH, Deerfield Beach, FL, 1985), pp. 236–259; H. Böttger and D. Wegner, in *Hopping and Related Phenomena*, edited by H. Fritzsche and M. Pollak (World Scientific, Singapore, 1990); H. Böttger, P. Szyler, and D. Wegener, *Phys. Status Solidi B* **128**, K179 (1985); **133**, K143 (1986).
- ³²E. I. Levin and B. I. Shklovskii, *Sov. Phys. Semicond.* **18**, 534 (1984).
- ³³B. I. Shklovskii, *Sov. Phys. Semicond.* **10**, 855 (1976).
- ³⁴N. F. Mott, *Metal-Insulator Transitions* (Taylor and Francis, London, 1974).
- ³⁵F. Zhang, A. Petr, H. Peisert, M. Knupfer, and L. Dunsch, *J. Phys. Chem. B* **108**, 17301 (2004).